MPC-Based Multi-Inverter Power Control in Low-Inertia Power Systems

Atinuke Ademola-Idowu and Baosen Zhang

***Abstract*—In a bid to make the electric grid more sustainable, there is a need to increase the integration of renewable energy resources at various locations in the grid. This move will reduce the total amount of physical inertia available from synchronous machines in the grid, resulting in the need for these resources to increasingly take on frequency response functions. In this paper, we propose a distributed model predictive based control method to coordinate multiple inverter-based resources in the grid. Under this control structure, the controller determines the optimal active power set-point for each inverter in the event of a disturbance in the system. In contrast to other control strategies, this controller does not constrain the inverters to behave like a traditional synchronous machine in responding to a disturbances. It instead leverages on the fast actuation of the inverters by virtue of the speed of its power electronic circuits. We demonstrate, by testing on the IEEE New England 39-bus system with integration of multiple inverter-based resources at different buses, that our proposed controller can coordinate these resources to provide an efficient frequency response under varying scenarios.**

2021 IEEE Power & Energy Society General Meeting (PESGM) | 978-1-6654-0507-2/21/$31.00 ©2021 IEEE | DOI: 10.1109/PESGM46819.2021.9638080

I. Introduction

Because of the drive to make the grid more sustainable and advancements in technology development of distributed energy resources, the amount of inverter-based resources (IBRs) integrated into the power system is projected to rise dramatically [1]. Since these IBRs are electronic devices and therefore lacking in physical inertia, there will be an accompanying decline in the available rotational inertia system-wide [2]. The lack of physical inertia by the IBRs can be compensated by their capability of injecting active power into the grid by the virtue of the speed of its power electronic circuits.

Varying control strategies that utilizes the IBRs as a means of compensating for the reduced inertia has been the subject of a lot of research in recent years (e.g., see [2], [3] and the references within), with the most popular being the *droop control* and *virtual synchronous machines* (VSMs). In their most basic forms, the frequency (angle) droop control injects/absorbs an amount of active power in proportion to the frequency deviation (relative phase angle) [4], [5], while the VSMs act as a second order oscillator to provide inertia and damping to the grid [6], [7].

A fundamental drawback of these control strategies is the constraining of IBRs to behave like synchronous machines when responding to a frequency event, as this ignores the fast action capability and the flexibility of the IBRs [8]. Also, during transient conditions where there are huge frequency variations across the network, with coherent groups of generators swinging against one another, using control strategies that utilize local information can result in the system going unstable [9]. This is due to either errors in estimating the true states or in some cases, the local information does not capture the true frequency dynamics of the whole network. Furthermore, in a network with multiple IBRs, due to their asynchronous nature, may require some form of coordination to ensure that the resources do not compete with each other in trying to provide frequency response. While adaptively changing the parameters of the controllers might improve its performance [10], it is still computationally difficult to compute these parameters in real-time. These parameters also depend on accurately determining system wide frequency deviations and rates of change of frequency (ROCOF), which local information cannot reliably provide.

Our previous work in [8] proposed a novel control strategy called the Inverter Power Control (IPC), based on model predictive control (MPC) algorithm. The IPC is used to optimally determine the active power set-point of an IBR, to minimize the frequency deviation and ROCOF. In the previous work, we assumed the IBRs integrated to the system can be aggregated into a single IBR. Realistically, this is not always so and running the IPC in a system with multiple IBRs can lead to these resources competing with each other, resulting in a poor frequency response. As the grid evolves, we expect to see more IBRs connected at different points in the grid and the question becomes how to coordinate these resources to jointly provide inertia compensation in the grid.

In this work, we extend the mathematical framework of the IPC, including its ability to handle hard constraints, to a multiple IBR system. We call this new controller the multi-inverter power control (MIPC). We show that by including a weighted IBR power output to the previously defined objective function, we are able to coordinate amongst multiple resources, to find the optimal active power set-point of the IBRs that minimizes the frequency deviation and ROCOF. We further show that the MPC algorithm is amenable to being used in a distributed control structure where each IBR utilizes state information from neighboring generators, by leveraging on an observer model and the synchronizing properties of the power system network, to estimate the unmeasured states and disturbances.

The remainder of this paper is organized as follows: Section II defines the models used in this paper. Section III presents the design and formulation of the MIPC algorithm. Section IV presents the distributed MIPC control. Section V shows the performances of MIPC in a centralized and distributed multiple IBR communication scenario. Section VI concludes the paper.

B. Zhang is with the Department of Electrical and Computer Engineering at the University of Washington, zhangbao@uw.edu. A. Ademola-Idowa is with GE Research, atinukeidowu@gmail.com. This work was partially supported by the NSF grant ECCS-1930605.

978-1-6654-0507-2/21/$31.00 ©2021 IEEE

II. Model

We denote the real numbers by $\mathbb{R}$, the cardinality of a set $\mathcal{S}$ as $|\mathcal{S}|$, the $n \times n$ identity and zero matrices as $\boldsymbol{I}_n$ and $\boldsymbol{0}_n$, respectively. Matrices and vectors are denoted by a bold-faced variables. Let the set of generators and IBRs be denoted by $\mathcal{G}$ and $\mathcal{I}$ respectively, such that the total number of generating sources in the network is $\mathcal{N} := \mathcal{G} \cup \mathcal{I}$.

A. Synchronous Machines

The rotor dynamics of each synchronous generator in a given power system is governed by the well-known swing equation [11]. Here we adopt a discretized version of the equations, which in per unit (p.u.) system is:

$$\begin{aligned} \omega_i^{t+1} &= \omega_i^t + \frac{h}{m_i}\left(P_{\mathrm{m},i}^t - P_{\mathrm{e},i}^t - d_i\omega_i^t\right) \ \forall i \in \mathcal{G} \\ \delta_i^{t+1} &= \omega_{\mathrm{b}}\left(\delta_i^t + h\ \omega_i^{t+1}\right) \ \forall i \in \mathcal{G}, \end{aligned} \tag{1}$$

where h is the step size for the discrete simulation, δ_i (rad) is the rotor angle, $\omega = \bar{\omega}_i - \omega_0$ is the rotor speed deviation, ω_{b} is the base speed of the system, m_i is the inertia constant, d_i is the damping constant, $P_{\mathrm{m},i}$ is the mechanical input power and $P_{\mathrm{e},i}$ is the electric power output of the i^{th} machine.

The electrical output power $P_{\mathrm{e},i}$ is given by the AC power flow equation in terms of the internal emf $|E_i|$ and rotor angle δ_i:

$$P_{\mathrm{e},i}^t = \sum_{i\sim j} |E_i E_j|[g_{ij}\cos(\delta_i^t - \delta_j^t) + b_{ij}\sin(\delta_i^t - \delta_j^t)], \tag{2}$$

$\forall i, j \in \mathcal{G}$, where $g_{ij} + jb_{ij}$ is the reduced admittance between nodes i and j. We assume the internal emf are constant because of the actions of the exciter systems.

B. Inverter Modeling

From the network point of view, the grid-connected IBRs is seen as producing a constant power according to its pre-determined set-point and fast dynamics governed by closed controls actions [12]. This helps the inverters maintain the output power, while remaining synchronized to the terminal voltage set by the grid. In order for an inverter to respond to a frequency deviation, an additional control loop, preferably one that does not alter the normal inverter operation, is needed to enable the inverters participate in frequency control. This can be achieved by changing the power set-point of the inverter based on frequency measurements.

III. Multi-Inverter Power Control (IPC)

In this work, we extend the performance of our proposed IBR output power control algorithm in [8] to handle scenarios where there are multiple IBRs connected at different points in the network. We term this extended controller a multi-inverter power controller (MIPC). This MIPC controller functions by modifying the initial real power set-points of all the IBRs in the network, that is from P_{0_k} to a new set-point P_{ref_k} as shown in Fig. 1. This new set-point is based not only on system state and network information, but also on the output power of the participating IBRs.

When dealing with multiple IBRs, the consideration of how the power imbalance response should be shared amongst the IBRs is needed. This power sharing capability amongst the IBRs can be incorporated into the control algorithm as a weighted minimization of the individual IBRs output power, noting that the IBR output power is a function of the system state and the IBR internal angle, as will be discussed later. This is somewhat similar in spirit to the droop configuration in synchronous machines where the individual droop settings of the machines determines how much power each machine contributes to the power imbalance in the network. This allows multiple machines work in tandem to share the responsibility of balancing out the power without competing each other [13]. The difference is that while the droop is a linear map between frequency and power output, the assigned weights here are not necessarily linear.

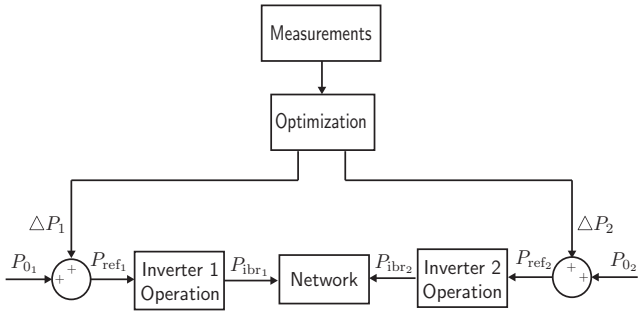

Fig. 1. Block Diagram showing the operation of the centralized MIPC controller which utilizes state and network information to modify the real power set-point of the IBRs at each timestep

A. Optimization Problem

The new MIPC optimization problem is obtained by adding a term that minimizes the weighted output power of the IBRs to the previously defined objective function, which minimizes a function of the frequency deviation and ROCOF. The MIPC optimization problem is formulated as follows:

$$\underset{\{\boldsymbol{u}^0,\boldsymbol{u}^1,\ldots,\boldsymbol{u}^{N-1}\}}{\text{Min.}} \ \sum_{t=0}^{N-1}\Big\{\|\boldsymbol{\omega}^{t+1}\|_2^2 + \frac{1}{h}\|\boldsymbol{\omega}^{t+1} - \boldsymbol{\omega}^t\|_2^2 \tag{3a}$$

$$+\|\boldsymbol{r} \odot \boldsymbol{P}_{\mathrm{ibr}}^t\|_2^2\Big\} \tag{3b}$$

$$\text{s.t. } \omega_i^{t+1} = \omega_i^t + \frac{h}{m_i}\big(P_{\mathrm{m},i}^t - P_{\mathrm{e},i}^t - d_i\omega_i^t - \triangle P_i^t\big), \ \forall i \in \mathcal{G} \tag{3c}$$

$$P_{e,i}^t = \text{Equation (2)}, \ \forall i \in \mathcal{G} \tag{3d}$$

$$P_{ibr,k}^t = \text{Equation (2)}, \ \forall k \in \mathcal{I} \tag{3e}$$

$$P_{\mathrm{ibr,min},k}^t \le P_{\mathrm{ibr},k}^t \le P_{\mathrm{ibr,max},k}^t, \tag{3f}$$

$$\sum_{t=1}^{N} P_{\mathrm{ibr,k}}^t \le E_{\mathrm{ibr,\ tot},k}^t, \tag{3g}$$

where $\boldsymbol{u}^t \in \mathcal{R}^{|\mathcal{I}|}$ is the vector of all IBR angles (referenced to the slack-bus) and represents the control variable in the optimization problem. $\boldsymbol{\omega}^{t+1} \in \mathcal{R}^{|\mathcal{G}|}$ is a vector of all machine frequency deviations at the next time step, $\boldsymbol{\omega}^{t+1} - \boldsymbol{\omega}^t$ is a vector of all machine ROCOF between the current and next time step. The evolution of $\boldsymbol{\omega}$ is given in (3c) (swing equations) with the added $\triangle P_i$ used to denote disturbances to the network which can be either a loss in generation or load. $\boldsymbol{P}_{\mathrm{e}}^t \in \mathcal{R}^{|\mathcal{G}|}$ and $\boldsymbol{P}_{\mathrm{ibr}}^t \in \mathcal{R}^{|\mathcal{I}|}$ are vectors of all generator and IBR output power respectively. Depending on how the system is interconnected, $\boldsymbol{P}_{\mathrm{ibr}}^t$ can also be written in the form of (2) [8]. The IBR droop

$\boldsymbol{r} \in \mathcal{R}^{|\mathcal{I}|}$ is a vector of weights for the IBRs output power and $\odot$ is the componentwise product between two vectors. The power and energy constraints are given in (3f) and (3g) respectively.

It should be noted that the actual control of the IBR is not done via angle control, rather, we use the optimized u_k to find the corresponding active power output of the IBR, then set the IBRs set-point to that power.

B. Model Predictive Control

The non-linearity of (2) makes (3) difficult to solve in real-time. To mitigate this, we linearize the swing equation in (3c) by using the standard DC power flow model, which is the linearized form of (2). The DC power flow can be written in a form that isolates the control variable (IBR angle) as follows:

$$\triangle P_e = \underbrace{\begin{bmatrix} b_{ii} & -b_{ij} \\ -b_{ji} & b_{jj} \end{bmatrix}}_{\boldsymbol{B}_{\text{GG}}} \begin{bmatrix} \triangle\delta_i \\ \triangle\delta_j \end{bmatrix} + \underbrace{\begin{bmatrix} -b_{ik} \\ -b_{jk} \end{bmatrix}}_{\boldsymbol{B}_{\text{GI}}} u_k, \tag{4}$$

where $\boldsymbol{B}_{\text{GG}}$ contains the connection between synchronous generators and $\boldsymbol{B}_{\text{GI}}$ contains the connection between a synchronous generator and IBRs.

Integrating (4) into (3c) and writing in matrix form results in:

$$\begin{aligned} \underbrace{\begin{bmatrix} \triangle\boldsymbol{\omega}^{\boldsymbol{t+1}} \\ \triangle\boldsymbol{\delta}^{\boldsymbol{t+1}} \end{bmatrix}}_{\boldsymbol{x^{t+1}}} &= \underbrace{\begin{bmatrix} -\boldsymbol{M^{-1}D} & -\boldsymbol{M^{-1}B}_{\text{GG}} \\ \boldsymbol{I_n} & \boldsymbol{0_n} \end{bmatrix}}_{\bar{\boldsymbol{A}}} \underbrace{\begin{bmatrix} \triangle\boldsymbol{\omega^t} \\ \triangle\boldsymbol{\delta^t} \end{bmatrix}}_{\boldsymbol{x^t}} \\ &+ \underbrace{\begin{bmatrix} -\boldsymbol{M^{-1}B}_{\text{GI}} \\ \boldsymbol{0_n} \end{bmatrix}}_{\bar{\boldsymbol{B}}_{\boldsymbol{u}}} \boldsymbol{u^t} + \underbrace{\begin{bmatrix} -\boldsymbol{M^{-1}} \\ \boldsymbol{0_n} \end{bmatrix}}_{\bar{\boldsymbol{B}}_{\boldsymbol{d}}} \underbrace{\triangle\boldsymbol{P^t}}_{\boldsymbol{d^t}} \end{aligned} \tag{5}$$

where $\triangle\boldsymbol{\delta} \in \mathbb{R}^n$ is the rotor angles deviation, $\triangle\boldsymbol{\omega} \in \mathbb{R}^n$ is the rotor speed deviation, $\boldsymbol{M} = diag(m_1, \ldots, m_n) \in \mathbb{R}^{n\times n}$, $\boldsymbol{D} = diag(d_1, \ldots, d_n) \in \mathbb{R}^{n\times n} \in \mathbb{R}^n$, $\triangle\boldsymbol{P} \in \mathbb{R}^n$ is vector of all power deviations which comes from the disturbances and noises in the system, denoted by $\boldsymbol{d}^t$.

To estimate the state and disturbance, as well as, model mismatches and other forms of disturbance, we first redefine $\boldsymbol{d^t}$ and $\bar{\boldsymbol{B}}_{\boldsymbol{d}}$ in (5) as a vector of all possible disturbances and some weighting matrix respectively. We then integrate the MIPC state space model in (5) with an input/output constant disturbance model [14] to obtain an augmented state space form as:

$$\begin{aligned} \underbrace{\begin{bmatrix} \boldsymbol{x^{t+1}} \\ \boldsymbol{d^{t+1}} \end{bmatrix}}_{\boldsymbol{z^{t+1}}} &= \underbrace{\begin{bmatrix} \bar{\boldsymbol{A}} & \bar{\boldsymbol{B}}_{\boldsymbol{d}} \\ \boldsymbol{0_n} & \boldsymbol{I_n} \end{bmatrix}}_{\boldsymbol{A}} \underbrace{\begin{bmatrix} \boldsymbol{x^t} \\ \boldsymbol{d^t} \end{bmatrix}}_{\boldsymbol{z^t}} + \underbrace{\begin{bmatrix} \bar{\boldsymbol{B}}_{\boldsymbol{u}} \\ \boldsymbol{0} \end{bmatrix}}_{\boldsymbol{B}} \boldsymbol{u^t} \\ \boldsymbol{y^t} &= \underbrace{\begin{bmatrix} \boldsymbol{I_{2n}} & \bar{\boldsymbol{C}}_{\boldsymbol{d}} \end{bmatrix}}_{\boldsymbol{C}} \underbrace{\begin{bmatrix} \boldsymbol{x^t} \\ \boldsymbol{d^t} \end{bmatrix}}_{\boldsymbol{z^t}}. \end{aligned} \tag{6}$$

where the disturbance $\boldsymbol{d^t}$ is modeled as a constant disturbance for the control period such that it follows an integral dynamics. The predicted augmented state and disturbance can then be estimated using the linear observer model as:

$$\hat{\boldsymbol{z}}^{\boldsymbol{t|t}} = \hat{\boldsymbol{z}}^{\boldsymbol{t|t-1}} + \underbrace{\begin{bmatrix} \boldsymbol{K_x} \\ \boldsymbol{K_d} \end{bmatrix}}_{\boldsymbol{K}} \left(\boldsymbol{y^t} - \boldsymbol{C}\hat{\boldsymbol{z}}^{\boldsymbol{t|t-1}}\right) \tag{7}$$

where $\boldsymbol{K}$ is the gain matrix for the augmented state and disturbance variable. For simplicity, we adopt a fixed gain structure for the gain matrix $\boldsymbol{K}$ with $\boldsymbol{K_x}$ and $\boldsymbol{K_d}$ chosen such that the estimator is stable.

With the model of the system defined and the ability to predict future evolution guaranteed, we reformulate the L2-norm objective function in (3a) in terms of the network model in (6).

For an unconstrained case, that is, the IPC optimization algorithm in (3) without the power limit constraint (3f) and total energy constraints (3g), the MPC is reduced to a linear quadratic programming (LQR) problem which can then be written for a N control horizon as:

$$J = \frac{1}{2}\hat{\boldsymbol{z}}^{\boldsymbol{0^T}}\boldsymbol{G}_{\text{mod}}\hat{\boldsymbol{z}}^{\boldsymbol{0}} + \frac{1}{2}\boldsymbol{u^T}\boldsymbol{H}_{\text{mod}}\boldsymbol{u} + \hat{\boldsymbol{z}}^{\boldsymbol{0^T}}\boldsymbol{F}_{\text{mod}}\boldsymbol{u}, \tag{8}$$

where $\boldsymbol{H}_{\text{mod}}$ and $\boldsymbol{F}_{\text{mod}}$ are constant matrices depending on $\boldsymbol{A}$ and $\boldsymbol{B}$ (See [15], Chapter 5 for more details).

For an infinite-horizon LQR problem, the optimal solution is linear in the starting point $\hat{\boldsymbol{z}}^0$ such that:

$$\boldsymbol{u^*} = -\boldsymbol{H}_{\text{mod}}^{\boldsymbol{-1}}\boldsymbol{F}_{\text{mod}}^{\boldsymbol{T}}\hat{\boldsymbol{z}}^{\boldsymbol{0}}. \tag{9}$$

In the presence of constraints, (8) becomes of the form.

$$\begin{aligned} \underset{\boldsymbol{u}}{\text{Min.}}\ & J = \frac{1}{2}\hat{\boldsymbol{z}}^{\boldsymbol{0^T}}\boldsymbol{G}_{\text{mod}}\hat{\boldsymbol{z}}^{\boldsymbol{0}} + \frac{1}{2}\boldsymbol{u^T}\boldsymbol{H}_{\text{mod}}\boldsymbol{u} + \hat{\boldsymbol{z}}^{\boldsymbol{0^T}}\boldsymbol{F}_{\text{mod}}\boldsymbol{u} \\ \text{s.t.}\ & \boldsymbol{Lu} \leq \boldsymbol{W} + \boldsymbol{V}\hat{\boldsymbol{z}}^{\boldsymbol{0}}, \end{aligned} \tag{10}$$

where $\mathbf{L}, \boldsymbol{W}$ and $\boldsymbol{V}$ depends on the constraint being considered. Equation (10) can no longer be solved as a linear programming problem but as a quadratic programming optimization problem with linear constraints.

In this paper, we consider constraints on the power output at each time step (3f) and constraints on the total energy available to provide frequency control (3g). Details on the structure of $\mathbf{L}, \boldsymbol{W}$ and $\boldsymbol{V}$ can be found in [8]

IV. Distributed MIPC

In a more realistic setting, especially in a large network where IBRs are interspersed, it might be difficult to get all state information to a central server and afterwards disperse to all IBRs. Under this setting, a form of distributed control strategy [16], [17] can be adopted where each IBR evaluates the same global objective function in the MIPC algorithm using the the network wide model and state information available to them, usually from a subset of the generators.

To achieve this, we assume at $t = 0$, the full state information is available to all IBRs after which we assume no further communication but instead rely on the synchronizing properties of the power systems [18]. It is well known that the frequencies of the synchronous machines are tightly coupled such that a disturbance to one generator is reflected across the network in the frequencies of the other generators [19]. At the next timestep, the IBR receives state information from a subset of generators and carries out an individual state and disturbance estimation using a reduced-order form of the augmented observer model in (7). Consider the operation of one of the IBRs $\mathcal{I}_k \in \mathcal{I}$ that receives state variable information from a subset of generators $\mathcal{G}_k \in \mathcal{G}$, where $|\mathcal{G}_k| = w$, such

that (6) and (7) becomes:

$$\underbrace{\begin{bmatrix}\hat{\boldsymbol{x}}_{\boldsymbol{k}}^{t|t}\\ \hat{\boldsymbol{d}}_{\boldsymbol{k}}^{t|t}\end{bmatrix}}_{\hat{\boldsymbol{z}}_{\boldsymbol{k}}^{t|t}} = \underbrace{\begin{bmatrix}\hat{\boldsymbol{x}}_{\boldsymbol{k}}^{t|t-1}\\ \hat{\boldsymbol{d}}_{\boldsymbol{k}}^{t|t-1}\end{bmatrix}}_{\hat{\boldsymbol{z}}_{\boldsymbol{k}}^{t|t-1}} + \underbrace{\begin{bmatrix}\boldsymbol{L}_{\boldsymbol{k_x}}\\ \boldsymbol{L}_{\boldsymbol{k_d}}\end{bmatrix}}_{\bar{L_k}} \left(\boldsymbol{y}_{\boldsymbol{k}}^{\boldsymbol{t}} - \begin{bmatrix}\boldsymbol{C} & \boldsymbol{C_d}\end{bmatrix} \begin{bmatrix}\hat{\boldsymbol{x}}_{\boldsymbol{k}}^{t|t-1}\\ \hat{\boldsymbol{d}}_{\boldsymbol{k}}^{t|t-1}\end{bmatrix} \right) \tag{11}$$

where $y_k^t \in \mathcal{R}^{2w}$ is the state information received from $\mathcal{G}_k$, and L_k is the augmented gain matrix for the k^{th} IBR such that $L_{k_x}, L_{k_d} \in \mathcal{R}^{m\times 2w}$. In this form, each IBR can then compute the MIPC algorithm in (8) by estimating the possible output of other IBRs and adjusting its output accordingly.

V. Results

In this section, we validate the performance of the MIPC controller by testing it on the IEEE New England 10-machine 39-bus (NE39) system used for power systems dynamics stability studies [20]. We study scenarios of up to four IBR integration into the network and of constraints on the power and energy output of the IBRs. Under each scenario, a large disturbance in form a partial generating capacity loss is applied to a generator in the network to initiate an event that can lead to a marked frequency decline.

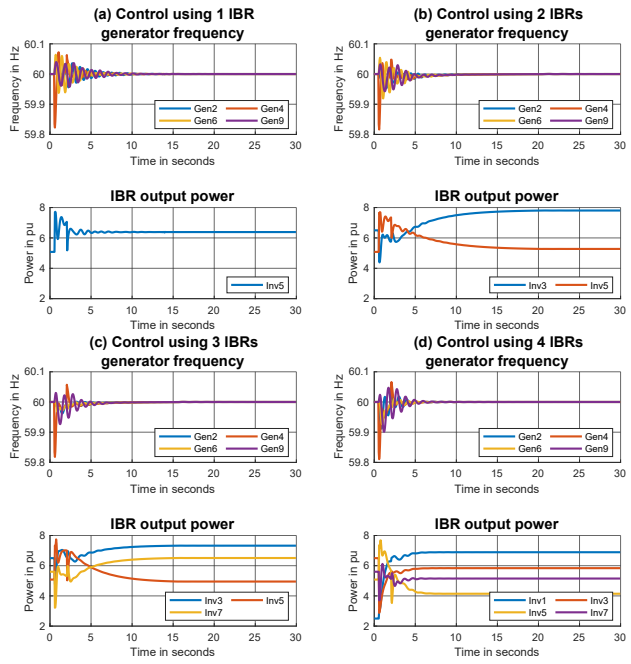

Fig. 2. Plot showing frequency response of some select generators and inverter output power using MIPC control strategy in an unconstrained scenario when multiple IBRs are integrated into the NE39 network. *(a)* One IBR connected as inv 5 at bus 34, *(b)* Two IBRs connected as inv 3 and 5 at bus 32 and 34 respectively, *(c)*: Three IBRs connected as inv 3, 5 and 7 at bus 32, 34 and 36 respectively, and *(d)*: Four IBRs connected as inv 1, 3, 5 and 7 at bus 30, 32, 34 and 36 respectively. The power output across the inverter is shared according to the weight assigned to each inverter.

The performance metrics for the MIPC controller is its ability to maintain the the frequency deviation within a small range, limiting the ROCOF, and quickly recovering to the nominal frequency value.

The NE39 network is transformed into a low-inertia network by removing the interconnection to the rest of the US network and replacing the generator at certain buses with IBRs (either solar or wind but coupled with energy storage) of aggregated capacity equalling that of the replaced generator, and reduced to an equivalent network using Kron reduction. The disturbance is applied to the fourth generator (*G4*) located at bus 33. Its power output starts of at 6.32pu, then decreases to 3.16pu at 0.5 seconds and later increases to 4.42pu at 2 seconds.

Under an unconstrained scenario, that is, under the conditions of unlimited IBR power and energy capacities, Fig. 2 shows the frequency response of select generators and inverter output power of the IBRs. For a clearer viewing, only the frequency response of the second (slack), fourth (disturbed), sixth and ninth generator are shown. When more than one IBR is integrated into the network, the MIPC is able to efficiently determine the optimal active power output of the individual IBR to ensure a suitable frequency response. The MIPC is able to share the total power response amongst the IBRs by weighting the output power of the IBRs similar to the way power output response is shared in a synchronous machine network. Furthermore, Fig. 2 shows that a better frequency response performance is obtained when using multiple IBRS as the frequency is able to return to its nominal value more quickly, with reduced oscillations as the number of IBRs increase, and the positive frequency deviation is reduced. In general, the MIPC controller is able to keep the frequency deviation within a 0.2Hz margin. The higher the number of IBRs the lower the amount of active power each IBR has to contribute.

Fig. 3 shows the frequency response of select generators and the inverter power outputs when two IBRs are integrated to the network, with a power limit of 7 pu and energy limit of 70 pu placed on the IBR (*inv 3*) connected at bus 32. In the power limit scenario, it can be observed that despite the limit on *inv 3*, the frequency response of the generators is the same as that of the unconstrained case in Fig. 2b, that is, about 0.2 Hz of negative deviation and about 0.05 Hz of positive deviation. In the energy limit scenario, the frequency response is slightly different from the unconstrained scenario in Fig. 2 as the positive deviation extends to about 0.1 Hz. Despite the limits, the MIPC is able to look ahead and also leverage on other IBR without an active constraint to ensure that the best strategy for an optimal frequency response is achieved.

Fig. 4 shows the frequency response of select generators and the inverter power outputs when two IBRs are integrated to the network under the modified distributed control scenario compared to a centralized control scenario. The observer model in the MIPC algorithm running on each IBR is able to estimate the unavailable states and disturbances, which is reflected as a mismatch between the available state measurement and the model predicted state. A combination of these estimates captures enough of the system level information to determine what the optimal power output of each inverter should be. It can also be observed that at the start of the disturbance, the inverter output power response initially varies significantly

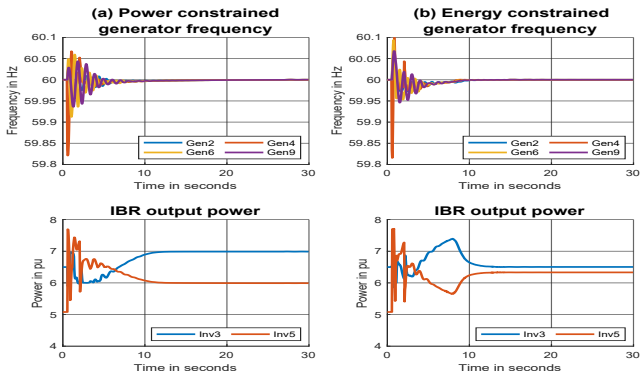

Fig. 3. Plot showing frequency response of some select generators and inverter output power using MIPC control strategy in a power and energy constrained scenario when two IBRs are integrated into the NE39 network. *LHS*: Power limit of *inv 3* constrained to 7 pu, and *RHS*: Total energy limit of *inv 3* constrained to 70 pu.

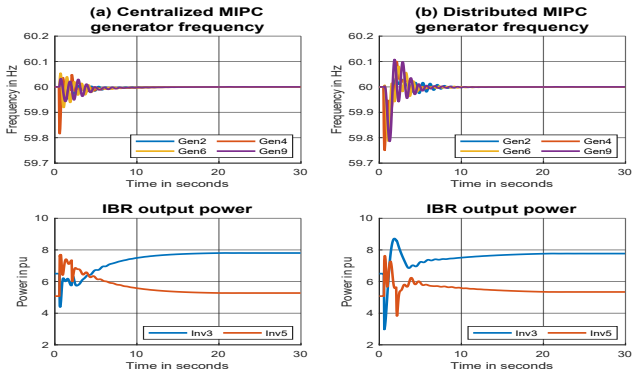

Fig. 4. Plot showing a comparison of the frequency response of some select generators and inverter output powers using MIPC control strategy in a centralized control scenario and a distributed control scenario when two IBRs are integrated into the NE39 network with each individual IBRs running MIPC control but don't communicate with each other.

compared to the centralized case and as a result, causes more initial deviation in frequency. The MIPC stabilizes the system afterwards and the output power settles to the same level as the centralized case.

We conjecture that the synchronizing properties of the electric grid [18] as well as its full connectivity enables the distributed MIPC controllers on each IBR to individually arrive at steady state conditions.

VI. Conclusion

In this paper, we extended the functionality of our previously proposed control strategy to handle coordination and control of multiple IBRs participating in frequency control at different locations in the grid, in both a centralized and distributed control scenario. We validated the performance of this controller on the IEEE 39-bus system and showed that its control performance does not deteriorate with the addition of more actuators, even under distributed control scenarios.

Future works will explore optimal placement of IBRs in a network because, as seen in the simulation results, this determines the significance of its participation in frequency control. Another next step is a theoretical stability guarantees, both in a centralized and distributed framework, especially in a network with strong interactions amongst the nodes due to the synchronizing properties of the power system structure.

References

[1] Bowman, Michelle, "Eia projects that renewables will provide nearly half of world electricity by 2050," https://www.eia.gov/todayinenergy/detail.php?id=41533, Oct 2019, [Online; accessed 05-April-2020].

[2] F. Milano, F. Dörfler, G. Hug, D. J. Hill, and G. Verbič, "Foundations and challenges of low-inertia systems," in *2018 Power Systems Computation Conference (PSCC)*. IEEE, 2018, pp. 1–25.

[3] U. Tamrakar, D. Shrestha, M. Maharjan, B. P. Bhattarai, T. M. Hansen, and R. Tonkoski, "Virtual inertia: Current trends and future directions," *Applied Sciences*, vol. 7, no. 7, p. 654, 2017.

[4] J. Van de Vyver, J. D. De Kooning, B. Meersman, L. Vandevelde, and T. L. Vandoorn, "Droop control as an alternative inertial response strategy for the synthetic inertia on wind turbines," *IEEE Transactions on Power Systems*, vol. 31, no. 2, pp. 1129–1138, 2015.

[5] R. Ofir, U. Markovic, P. Aristidou, and G. Hug, "Droop vs. virtual inertia: Comparison from the perspective of converter operation mode," in *2018 IEEE International Energy Conference (ENERGYCON)*. IEEE, 2018.

[6] K. Sakimoto, Y. Miura, and T. Ise, "Stabilization of a power system with a distributed generator by a virtual synchronous generator function," in *Power Electronics and ECCE Asia (ICPE & ECCE), 2011 IEEE 8th International Conference on*. IEEE, 2011, pp. 1498–1505.

[7] A. Ademola-Idowu and B. Zhang, "Optimal design of virtual inertia and damping coefficients for virtual synchronous machines," in *Power and Energy Society General Meeting*, 2018.

[8] ——, "Frequency stability using inverter power control in low-inertia power systems," *IEEE Transactions on Power Systems*, 2020.

[9] E. Rakhshani and P. Rodriguez, "Inertia emulation in ac/dc interconnected power systems using derivative technique considering frequency measurement effects," *IEEE Transactions on Power Systems*, vol. 32, no. 5, pp. 3338–3351, 2016.

[10] F. Wang, L. Zhang, X. Feng, and H. Guo, "An adaptive control strategy for virtual synchronous generator," *IEEE Transactions on Industry Applications*, vol. 54, no. 5, pp. 5124–5133, 2018.

[11] P. W. Sauer, M. Pai, and J. H. Chow, *Power system dynamics and stability: with synchrophasor measurement and power system toolbox*. John Wiley & Sons, 2017.

[12] H. N. V. Pico and B. B. Johnson, "Transient stability assessment of multi-machine multi-converter power systems," *IEEE Transactions on Power Systems*, 2019.

[13] P. Kundur, "Power system control and stability," *New York: McGraw*, 1994.

[14] G. Pannocchia and J. B. Rawlings, "Disturbance models for offset-free model-predictive control," *AIChE journal*, vol. 49, no. 2, pp. 426–437, 2003.

[15] A. A. Ademola-Idowu, "Frequency stability in low-inertia power systems," Ph.D. dissertation, University of Washington, 2020.

[16] E. Camponogara, D. Jia, B. H. Krogh, and S. Talukdar, "Distributed model predictive control," *IEEE control systems magazine*, vol. 22, no. 1, pp. 44–52, 2002.

[17] B. T. Stewart, A. N. Venkat, J. B. Rawlings, S. J. Wright, and G. Pannocchia, "Cooperative distributed model predictive control," *Systems & Control Letters*, vol. 59, no. 8, pp. 460–469, 2010.

[18] F. Dorfler and F. Bullo, "Synchronization and transient stability in power networks and nonuniform kuramoto oscillators," *SIAM Journal on Control and Optimization*, vol. 50, no. 3, pp. 1616–1642, 2012.

[19] J. Machowski, J. Bialek, and J. Bumby, *Power system dynamics: stability and control*. John Wiley & Sons, 2011.

[20] R. Ramos, I. Hiskens *et al.*, "Benchmark systems for small-signal stability analysis and control," *IEEE Power and Energy Society*, 2015.